

Point RCNN: An Angle-Free Framework for Rotated Object Detection

Qiang Zhou,^{*} Chaohui Yu,^{*} Zhibin Wang,[†] Hao Li
Alibaba Group

{jianchong.zq, huakun.ych, zhibin.waz, lihao.lh}@alibaba-inc.com

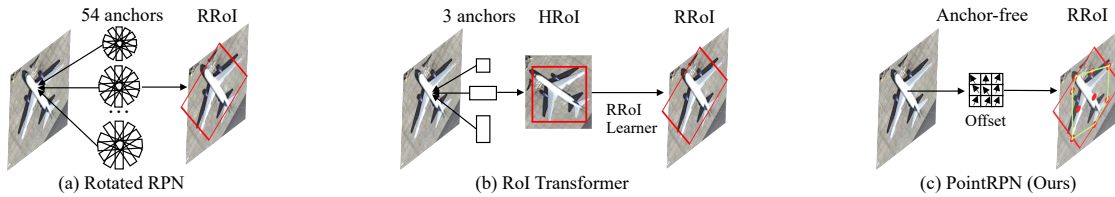


Figure 1. Comparison of different methods for generating rotated RoI (RRoI). (a) Rotated RPN places multiple rotated anchors with different angles, scales, and aspect ratios. (b) RoI Transformer proposes a RRoI learner to model the RRoI from the horizontal RoI (HRoI) for each feature point based on 3 anchors. (c) Our proposed PointRPN generates accurate RRoI in an anchor-free and angle-free manner.

Abstract

Rotated object detection in aerial images is still challenging due to arbitrary orientations, large scale and aspect ratio variations, and extreme density of objects. Existing state-of-the-art rotated object detection methods mainly rely on angle-based detectors. However, angle regression can easily suffer from the long-standing boundary problem. To tackle this problem, we propose a purely angle-free framework for rotated object detection, called Point RCNN, which mainly consists of PointRPN and PointReg. In particular, PointRPN generates accurate rotated RoIs (RRoIs) by converting the learned representative points with a coarse-to-fine manner, which is motivated by RepPoints. Based on the learned RRoIs, PointReg performs corner points refinement for more accurate detection. In addition, aerial images are often severely unbalanced in categories, and existing methods almost ignore this issue. In this paper, we also experimentally verify that re-sampling the images of the rare categories will stabilize training and further improve the detection performance. Experiments demonstrate that our Point RCNN achieves the new state-of-the-art detection performance on commonly used aerial datasets, including DOTA-v1.0, DOTA-v1.5, and HRSC2016.

^{*}These authors contributed equally to this work.

[†]Corresponding author.

1. Introduction

Although object detection has achieved significant progress in natural images, it still remains challenging for rotated object detection in aerial images, due to the arbitrary orientations, large scale and aspect ratio variations, and extreme density of objects [40]. Rotated object detection aims at predicting a set of oriented bounding box (OBB) and the corresponding classes in an aerial image, which has been serving as an essential step in many applications, *e.g.*, urban management, emergency rescue, precise agriculture [9]. Modern rotated object detectors can be divided into two categories in terms of the representation of OBB: angle-based detectors and angle-free detectors.

In angle-based detectors, an OBB of a rotated object is usually represented as a five-parameter (x, y, w, h, θ) . Most existing state-of-the-art methods are angle-based detectors relying on two-stage RCNN frameworks [8, 16, 20, 41, 48]. Generally, these methods use an RPN to generate horizontal or rotated RoIs, then use a designed RoI pooling operator to extract features from these RoIs. Finally, an RCNN head is used to predict the OBB and the corresponding classes. Compared to two-stage detectors, one-stage angle-based detectors [15, 31, 44, 45, 52] directly regress the OBB and classify them based on dense anchors for efficiency.

However, angle-based detectors usually introduce a long-standing boundary discontinuity problem [43, 47] due to the periodicity of angle and exchange of edges. Moreover, the unit between (x, y, w, h) and angle θ of the five-parameter representation is not consistent. These obstacles will cause the training unstable and limit the performance.

In contrast with angle-based detectors, angle-free detectors usually represent a rotated object as an eight-parameter OBB $(x_1, y_1, x_2, y_2, x_3, y_3, x_4, y_4)$, which denotes the four corner points of a rotated object. Modern angle-free detectors [1, 33, 42, 51] directly perform quadrilateral regression, which is more straightforward than the angle-based representation. Unfortunately, although abandoning angle regression and the parameter unit is consistent as well, the performance of existing angle-free detectors is still relatively limited. How to design a more straightforward and effective framework to alleviate the boundary discontinuity problem is the key to the success of rotated object detectors.

In this paper, we propose a purely angle-free framework for rotated object detection, called Point RCNN, which can alleviate the boundary discontinuity problem and attain state-of-the-art performance. Concretely, Point RCNN is a two-stage detector and mainly consists of an RPN (PointRPN) and an RCNN head (PointReg), which are both angle-free. Given an input feature map, first, PointRPN learns a set of representative points for each feature point with a coarse-to-fine manner. Then, rotated RoI (RRoI) is generated through the `MinAreaRect` function of OpenCV [2]. Finally, PointReg applies a rotate RoI Align [8, 16] operator to extract RRoI features, and then refines and classifies the eight-parameter OBB of corner points. In addition, the existing methods almost ignore the category imbalance in aerial images, and we propose to resample images of rare categories to stabilize convergence during training.

The contributions of this paper are as follows:

- We propose Point RCNN, a purely angle-free framework for rotated object detection. Without introducing angle prediction, Point RCNN is able to address the boundary discontinuity problem.
- We propose PointRPN and PointReg to reformulate angle prediction as the more straightforward points regression. Both of them are angle-free and have consistent parameter units. We further propose to resample images of rare categories to stabilize training and improve overall performance.
- Compared with the state-of-the-art methods, our Point RCNN framework attains higher detection performance on several large-scale datasets.

2. Related Work

2.1. Horizontal Object Detection

In the past decade, object detection has become an important computer vision task and has received considerable attention. One line of research focuses on two-stage detectors [3, 11, 12, 17, 18, 25, 35], which first generates a

sparse set of Regions of Interests (RoI) with a Region Proposal Network (RPN), and then performs classification and bounding box regression. While two-stage detectors still attract much attention, another line of research tends to develop efficient one-stage detectors [10, 22, 26, 28, 34, 37, 50], in which SSD [28] and YOLO [34] are the fundamental methods that use a set of pre-defined anchor boxes to predict object category and anchor box offsets. Recently, some anchor-free methods [10, 22, 50] detect object by predicting the center or corner or representative points, which also inspire us to develop the angle-free detector for rotated object.

2.2. Rotated Object Detection

In terms of the representation of oriented bounding box (OBB), modern rotated object detectors can be mainly divided into two categories: angle-based detectors and angle-free detectors.

Angle-based detectors detect rotated object by learning a five-parameter OBB (x, y, w, h, θ) , in which (x, y, w, h) denotes a horizontal bounding box and θ denotes the rotated angle between the longer edge and the horizontal axis. RRPNN [31] and R²PN [52] make use of multiple rotated anchors with different angles, scales, and aspect ratios, which improves the performance while increasing the computational complexity (see Fig. 1(a)). R²CNN [20] proposes to detect horizontal and rotated bounding box simultaneously with multi task learning. RoI Transformer [8] proposes a rotated RoI (RRoI) learner to transform a horizontal RoI into a RRoI, which provides more accurate RRoIs with a complex pipeline (see Fig. 1(b)). SCRDet [48] enhances features with attention module and proposes an IoU-smooth L_1 loss to alleviate the loss discontinuity issue. CSL [45] reformulates angle prediction from regression to classification to alleviate discontinuous boundary problem. GWD [46] and KLD [49] propose more efficient loss function for OBB regression. S²A-Net [15] proposes a single-shot alignment network to realize full feature alignment and alleviates the inconsistency between regression and classification. Recently, ReDet [16] proposes to use rotation-equivariant network to encode rotation equivariance explicitly and presents rotation-invariant RoI Align to extract rotation-invariant features. Oriented R-CNN [41] proposes a two-stage detector that consists of an oriented RPN for generating RRoI and an oriented RCNN for refining the RRoI. Both ReDet and Oriented RCNN provide promising accuracy.

However, the boundary problem in the angle regression learning still causes training unstable and limits the performance. While angle-based detectors still find many applications, angle-free methods are getting more and more attention from the community.

Angle-free detectors reformulate rotated object

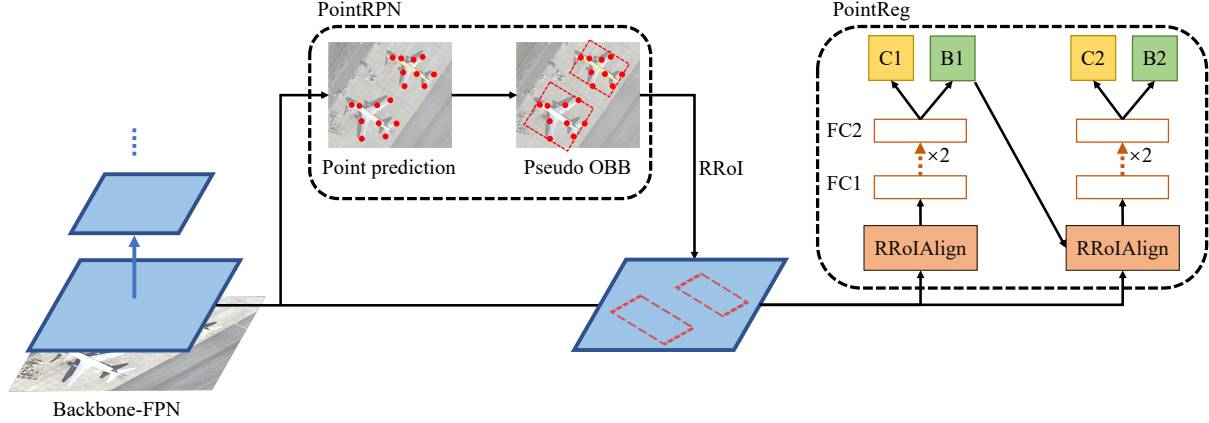


Figure 2. The proposed angle-free Point RCNN framework for rotated object detection. Point RCNN mainly consists of two modules: PointRPN for generating rotated proposals, and PointReg for refining for more accurate detection. “RRoI” denotes rotated RoI, “FC” denotes fully-connected layer, “C” and “B” represent the predicted category and rotated box coordinates of each RRoI, respectively.

regression as learning a eight-parameter OBB $(x_1, y_1, x_2, y_2, x_3, y_3, x_4, y_4)$, which represents the four corner points of a rotated object. ICN [1] proposes to directly estimate the four vertices of a quadrilateral to regress an oriented object based on image pyramid and feature pyramid. RSDet [33] and Gliding Vertex [42] achieve more accurate rotated object detection via directly quadrilateral regression prediction. Recently, BBAVectors [51] extends the horizontal keypoint-based object detector to the oriented object detection task. CFA [13] proposes a convex-hull feature adaptation approach for configuring convolutional features. Compared to angle-based methods, angle-free detectors are more straightforward and can alleviate the boundary problem to a large extent. However, the performance is relatively limited yet.

In this paper, we propose an effective angle-free framework for rotated object detection, *i.e.*, Point RCNN, which mainly consists of PointRPN and PointReg. Compared with other RRoI generation methods, our PointRPN generates accurate RRoI in an anchor-free and angle-free manner (see Fig. 1(c)).

3. Point RCNN

The overall structure of our Point RCNN is depicted in Fig. 2. We start by revisiting the boundary discontinuity problem of angle-based detectors. Then, we describe the overall pipeline of Point RCNN. Finally, we elaborate the PointRPN and PointReg modules, and propose a balanced dataset strategy to rebalance the long-tailed datasets during training.

3.1. Boundary Discontinuity

Boundary problem [43, 47] is a long-standing problem that existed in angle-based detectors. Take the commonly used five-parameter OBB representation (x, y, w, h, θ) as

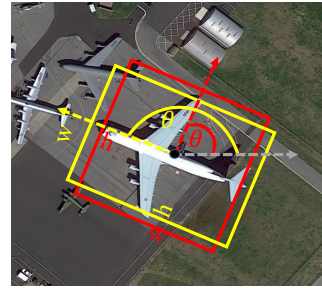


Figure 3. Boundary discontinuity problem of angle prediction. Red and yellow indicate two different targets.

an example, where (x, y) represents the center coordinates, (w, h) represents the shorter and longer edges of the box, and θ represents the angle between the longer edge and the horizontal axis. As shown in Fig. 3, when the target box is approximately square, a slight variation in edge length may cause w and h to swap, leading to a substantial variation of $\pi/2$ in angle θ .

This boundary discontinuity issue in angle prediction will confuse the optimization of the network and limit the detection performance.

3.2. Overview

The overall pipeline of Point RCNN is shown in Fig. 2. During training, Backbone-FPN first extracts feature maps given an input image. Then, PointRPN performs representative points regression and generates pseudo OBB for rotated RoI (RRoI). Finally, for each RRoI, PointReg refines the corner points and classifies them for final detection results. Besides, we propose to resample images of rare categories to stabilize training and improve the overall performance.

The overall training objective is described as:

$$\mathcal{L} = \mathcal{L}_{PointRPN} + \mathcal{L}_{PointReg}, \quad (1)$$

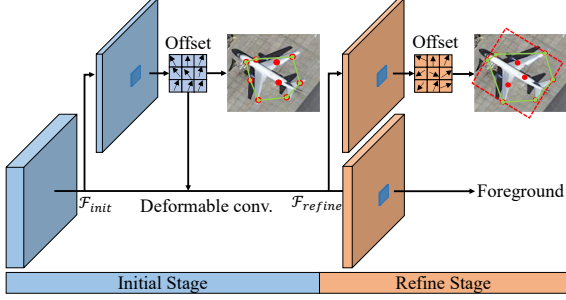


Figure 4. The structure of the proposed PointRPN. The red points are the learned representative points, and the green polygon represents the converted convex-hull. The red dotted OBB is converted from the representative points with the `MinAreaRect` function of OpenCV [2] for generating RRoI.

where $\mathcal{L}_{PointRPN}$ denotes the losses in PointRPN, and $\mathcal{L}_{PointReg}$ denotes the losses in PointReg. We will describe them in detail in the following sections.

3.3. PointRPN

Existing rotated object detection methods generate rotated proposals indirectly by transforming the outputs of RPN [36] and suffer from the boundary discontinuity problem caused by angle prediction. For example, [8, 16] use RoI transformer to convert horizontal proposals to rotated proposals with an additional angle prediction task. Unlike these methods, in this paper, we propose to directly predict the rotated proposals with representative points learning. The learning of points is more flexible, and the distribution of points can reflect the angle and size of the rotated object. The boundary discontinuity problem can thus be alleviated without angle regression.

Representative Points Prediction. Inspired by Rep-Points [50] and CFA [13], we propose PointRPN to predict the representative points in the RPN stage. The predicted points can effectively represent the rotating box and can be easily converted to rotated proposals in subsequent RCNN stages.

As shown in Fig. 4, PointRPN learns a set of representative points for each feature point. In order to make the features better adapt to the representative points learning, we take a coarse-to-fine prediction manner. In this way, the features will be refined with DCN [7] and the predicted offset in the initial stage. For each feature point, the predicted representative points of the two stages are:

$$\begin{aligned} \mathcal{R}^{init} &= \{(x_i^0 + \Delta x_i^0, y_i^0 + \Delta y_i^0)\}_{i=1}^K, \\ \mathcal{R}^{refine} &= \{(x_i^1 + \Delta x_i^1, y_i^1 + \Delta y_i^1)\}_{i=1}^K, \end{aligned} \quad (2)$$

where K denotes the number of predicted representative points and we set $K = 9$ by default. $\{(x_i^0, y_i^0)\}_{i=1}^K$ denotes the initial location, $\{(\Delta x_i^0, \Delta y_i^0)\}_{i=1}^K$ denote the learned

offsets in the initial stage, and $\{(\Delta x_i^1, \Delta y_i^1)\}_{i=1}^K$ denote the learned offsets in the refine stage.

Label Assignment. PointRPN predicts representative points for each feature point in the initial and refine stages. This section will describe how we determine the positive samples among all feature points for these two stages.

For the initial stage, we project each ground-truth box to the corresponding feature level according to its area, and then select the feature point closest to its center as the positive sample. The rule used for projecting the ground-truth box b_i^* to the corresponding feature level is defined as:

$$l_i = \log_2 \left(\sqrt{\frac{w_i h_i}{s}} \right), \quad (3)$$

where s is a hyper-parameter and is set to 16 by default. w_i and h_i are the width and height of b_i^* .

For the refine stage, we use the predicted representative points from the initial stage to help determine the positive samples. Specifically, for each feature point with its corresponding prediction \mathcal{R}^{init} , if the maximum convex-hull IoU (defined in Eq. (6)) between \mathcal{R}^{init} and ground-truth boxes exceeds the threshold τ , we select this feature point as a positive sample. We set $\tau = 0.1$ in all our experiments.

Optimization. The optimization of the proposed PointRPN is driven by classification loss and rotated object localization loss. The learning objective is formulated as:

$$\mathcal{L}_{PointRPN} = \lambda_1 + \mathcal{L}_{loc}^{init} + \lambda_2 \mathcal{L}_{cls}^{refine} + \lambda_3 + \mathcal{L}_{loc}^{refine}, \quad (4)$$

where λ_1, λ_2 , and λ_3 are the trade-off parameters and are set to 0.5, 1.0, and 1.0 by default, respectively. $+\mathcal{L}_{loc}^{init}$ denotes the localization loss of the initial stage. $\mathcal{L}_{cls}^{refine}$ and $+\mathcal{L}_{loc}^{refine}$ denote the classification loss and localization loss of the refine stage. Note that the classification loss is only calculated in the refine stage, and the two localization losses are only calculated for the positive samples.

In the initial stage, the localization loss is conducted between the convex-hulls converted from the learned points \mathcal{R}^{init} (see initial stage in Fig. 4) and the ground-truth OBBs. We use convex-hull GIoU loss [13] to calculate the localization loss:

$$+\mathcal{L}_{loc}^{init} = \frac{1}{N_{pos}^0} \sum_i \left(1 - \text{CIoU}(\Gamma(\mathcal{R}_i^{init}), \Gamma(b_i^*)) \right), \quad (5)$$

where N_{pos}^0 indicates the number of positive samples of the initial stage. b_i^* is the matched ground-truth OBB. CIoU represents the convex-hull GIoU between the two convex-hulls $\Gamma(\mathcal{R}_i^{init})$ and $\Gamma(b_i^*)$, which is differential and can be

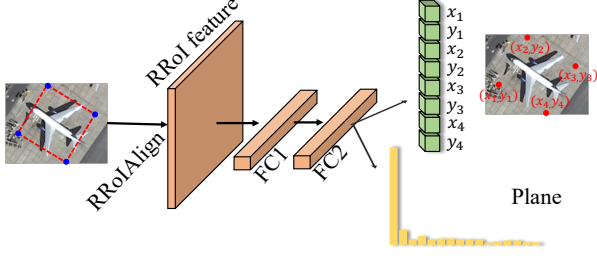


Figure 5. The diagram of the proposed PointReg. For simplicity, we only show the first stage of PointReg. Blue and red points denote the four corner points of the input RRoI and the refined results, respectively.

calculated as:

$$\text{CIoU}(\Gamma(\mathcal{R}_i^{init}), \Gamma(b_i^*)) = \frac{|\Gamma(\mathcal{R}_i^{init}) \cap \Gamma(b_i^*)|}{|\Gamma(\mathcal{R}_i^{init}) \cup \Gamma(b_i^*)|} - \frac{|\mathcal{P}_i \setminus (\Gamma(\mathcal{R}_i^{init}) \cup \Gamma(b_i^*))|}{\mathcal{P}_i}, \quad (6)$$

where the first term denotes the convex-hull IoU, and \mathcal{P}_i denotes the smallest enclosing convex object area of $\Gamma(\mathcal{R}_i^{init})$ and $\Gamma(b_i^*)$. $\Gamma(\cdot)$ denotes the Jarvis March algorithm [19] used to calculate the convex-hull from points.

The learning of the refine stage, which is responsible for outputting more accurate rotated proposals, is driven by both classification loss and localization loss. $\mathcal{L}_{cls}^{refine}$ is a standard focal loss [26], which can be calculated as:

$$\mathcal{L}_{cls}^{refine} = \frac{1}{N_{pos}^1} \sum_i \text{FL}(p_i, c_i^*), \quad (7)$$

$$\text{FL}(p_i, c_i^*) = \begin{cases} -\alpha(1-p_i)^\gamma \log(p_i), & \text{if } c_i^* > 0; \\ -(1-\alpha)p_i^\gamma \log(1-p_i), & \text{otherwise,} \end{cases} \quad (8)$$

where N_{pos}^1 denotes the number of positive samples in the refine stage, p_i and c_i^* are the classification output and the assigned ground-truth category, respectively. α and γ are hyper-parameters and are set to 0.25 and 2.0 by default. The localization loss $\mathcal{L}_{loc}^{refine}$ is similar to Eq. (5) and can be formulated as:

$$+\mathcal{L}_{loc}^{refine} = \frac{1}{N_{pos}^1} \sum_i \left(1 - \text{CIoU}(\Gamma(\mathcal{R}_i^{refine}), \Gamma(b_i^*))\right). \quad (9)$$

With the refined representative points, pseudo OBB is converted using the `MinAreaRect` function of OpenCV [2], which is then used for generating RRoI for PointReg.

As illustrated in Fig. 6, our PointRPN can automatically learn extreme points and semantic key points of rotated objects.

3.4. PointReg

Corner Points Refine. The rotated proposals generated by

PointRPN already provide a reasonable estimate for the target rotated objects. To avoid the problems caused by angle regression and further improve the performance, we turn to refine the four corners of the rotated proposals in the RCNN stage. As shown in Fig. 5, with the rotated proposals as input, we use a RRoI feature extractor [8, 16] to extract RRoI features. Then, given the RRoI features, two consecutive fully-connected and ReLU layers are used to encode the RRoI features. Finally, two fully-connected layers are responsible for predicting the class probability P and refined corners \mathcal{C} of the corresponding rotated object. The refined corners are represented as:

$$\mathcal{C} = \{(x_i + \Delta x_i, y_i + \Delta y_i)\}_{i=1}^4, \quad (10)$$

where $\{(x_i, y_i)\}_{i=1}^4$ denotes the corner coordinates of the input rotated proposals. $\{(\Delta x_i, \Delta y_i)\}_{i=1}^4$ denotes the predicted corner offsets.

Instead of directly performing angle prediction, we refine the four corners of the input rotated proposals. There are three advantages of adopting corner points refinement: 1). it can alleviate the boundary discontinuity problem caused by angle prediction; 2). the parameter units are consistent among the eight parameters; 3). it is possible to improve the localization accuracy using a coarse-to-fine manner.

We can easily extend PointReg to cascade structure for better performance. As shown in Fig. 2, in the cascade structure, the refined rotated proposals of the previous stage are used as the input of the current stage.

Optimization. The learning of PointReg is driven by classification loss and rotated object localization loss:

$$\mathcal{L}_{PointReg} = \mu_1 \mathcal{L}_{cls} + \mu_2 + \mathcal{L}_{loc}, \quad (11)$$

where μ_1 and μ_2 are the trade-off coefficients and are both set to 1.0 by default. \mathcal{L}_{cls} indicates the classification loss, which is a cross-entropy loss:

$$\mathcal{L}_{cls} = -\frac{1}{N} \sum_i \sum_{c=0}^C Y_{i \rightarrow c} \log(P_i), \quad (12)$$

where N denotes the number of training samples in PointReg, C is the number of categories excluding background, P_i is the predicted classification probability of the i th RRoI. $Y_{i \rightarrow c} = 1$ if the ground-truth class of the i th RRoI is c ; otherwise it is 0. $+\mathcal{L}_{loc}$ represents the localization loss between the refined corners and the corners of ground-truth OBB. We use L_1 loss to optimize the corner refinement learning:

$$+\mathcal{L}_{loc} = \frac{1}{N} \sum_i |C_i - \vartheta(b_i^*)|, \quad (13)$$

where $\mathcal{C}_i (= \{(x_j, y_j)\}_{j=1}^4)$ denotes refined corners for the i_{th} rotated proposal, $b_i^* (= \{(x_j^*, y_j^*)\}_{j=1}^4)$ denotes the corners of matched ground-truth OBB. $\vartheta(b_i^*)$ denotes the permutation of four corners of b_i^* with the smallest L_1 loss $|\mathcal{C}_i - \vartheta(b_i^*)|$. Note that $+\mathcal{L}_{loc}$ is only calculated for positive training samples.

3.5. Balanced Dataset

The extremely nonuniform object densities of aerial images usually make the dataset long-tailed, which may cause the training process to be unstable and limit the detection performance. For instance, DOTA-v1.0 contains 52, 516 ship instances but only 678 ground track field instances [9]. To alleviate this issue, we resample the images of rare categories, which is inspired by [14]. More concretely, first, for each category $c \in C$, compute the fraction of images F_c that contains this category. Then, compute the category-level repeat factor for each category:

$$r_c = \max(1.0, \sqrt{\beta_{thr}/F_c}), \quad (14)$$

where β_{thr} is a threshold which indicates that there will be not oversampling if “ $F_c > \beta_{thr}$ ”. Finally, compute the image-level repeat factor r_I for each image I :

$$r_I = \max_{c \in C_I}(r_c), \quad (15)$$

where C_I denotes the categories contained in I . In other words, those images that contain long-tailed categories will have a greater chance of being resampled during training.

4. Experiment

4.1. Datasets

To evaluate the effectiveness of our proposed Point RCNN framework, we perform experiments on two popular large-scale datasets: DOTA [40] and HRSC2016 [30].

DOTA [40] is the largest dataset for oriented object detection with three released versions: DOTA-v1.0, DOTA-v1.5 and DOTA-v2.0. To compare the performance with the state-of-the-art methods, we perform experiments on DOTA-v1.0 and DOTA-v1.5. DOTA-v1.0 contains 2806 images ranging in size from 800×800 to 4000×4000 , and contains 188, 282 instances in 15 categories: Bridge (BR), Harbor (HA), Ship (SH), Plane (PL), Helicopter (HC), Small vehicle (SV), Large vehicle (LV), Baseball diamond (BD), Ground track field (GTF), Tennis court (TC), Basketball court (BC), Soccer-ball field (SBF), Roundabout (RA), Swimming pool (SP), and Storage tank (ST). DOTA-v1.5 has the same images as DOTA-v1.0 but contains 402, 089 instances. This is a more challenging dataset, which introduces a new category Container Crane (CC) and more small instances.

HRSC2016 [30] contains 1061 aerial images with size ranges from 300×300 to 1500×900 . There are 436, 181, and 444 images in the training, validation and test set, respectively.

4.2. Implementation Details

We implement Point RCNN using the MMDetection tool-box [6]. We follow ReDet [16] to use ReResNet with ReFPN as our backbone (ReR50-ReFPN), which has shown the ability to extract rotation-equivariant features. We also verify with the more generalized transformer backbone (Swin-Tiny) to show the generalization and scalability of our Point RCNN.

On the DOTA dataset, following previous methods [8, 15, 16], we crop the image to 1024×1024 with 824 pixels as a stride and we also resize the image to three scales $\{0, 5, 1.0, 1.5\}$ for multi-scale data. Random horizontal flipping and random rotation ($[-45^\circ, 45^\circ]$) are adopted for multi-scale training. On the HRSC2016 dataset, like previous method [16], we resize all the images to (800, 512), random horizontal flipping is applied during training. Unless otherwise specified, we train all the models with 19 epochs for DOTA and 36 epochs for HRSC2016. To be specific, we train the models using AdamW [21] on 8 Tesla-V100 GPUs with $\beta_1=0.9$ and $\beta_2=0.999$, with an initial learning rate of 0.0002, a weight decay of 0.05, and a mini-batch size of 16 (2 images per GPU). The learning rate decays by a factor of 10 at each decay step.

4.3. Main Results

We compare our Point RCNN framework with other state-of-the-art methods on three datasets: DOTA-v1.0, DOTA-v1.5, and HRSC2016. As shown in Tab. 1, Tab. 2, and Tab. 3, without bells and whistles, our Point RCNN demonstrates superior performance against state-of-the-art methods.

On DOTA-v1.0, as reported in Tab. 1, Point RCNN achieves state-of-the-art **80.71** mAP. With the more generalized transformer backbone Swin-Tiny [29] (Swin-T), Point RCNN can further improve the performance by **0.61%** (from 80.71 to 81.32).

On DOTA-v1.5, which is more challenging compared to DOTA-v1.0, Point RCNN achieves **79.31** mAP, which significantly improve the performance by **2.51%**. With the more generalized transformer backbone Swin-T, Point RCNN further improves the performance by **0.83%** (from 79.31 to 80.14). The results are reported in Tab. 2

On HRSC2016, as reported in Tab. 3, Point RCNN attains the new state-of-the-art performance under both the VOC2007 and VOC2012 metrics, respectively.

Method	Backbone	PL	BD	BR	GTF	SV	LV	SH	TC	BC	ST	SBF	RA	HA	SP	HC	mAP (%)
RoI Trans.* [8]	R101-FPN	88.64	78.52	43.44	75.92	68.81	73.68	83.59	90.74	77.27	81.46	58.39	53.54	62.83	58.93	47.67	69.56
O ² -DNet* [39]	H104	89.30	83.30	50.10	72.10	71.10	75.60	78.70	90.90	79.90	82.90	60.20	60.00	64.60	68.90	65.70	72.80
DRN* [32]	H104	89.71	82.34	47.22	64.10	76.22	74.43	85.84	90.57	86.18	84.89	57.65	61.93	69.30	69.63	58.48	73.23
Gliding Vertex* [42]	R101-FPN	89.64	85.00	52.26	77.34	73.01	73.14	86.82	90.74	79.02	86.81	59.55	70.91	72.94	70.86	57.32	75.02
BBAVectors* [51]	R101	88.63	84.06	52.13	69.56	78.26	80.40	88.06	90.87	87.23	86.39	56.11	65.62	67.10	72.08	63.96	75.36
CenterMap* [38]	R101-FPN	89.83	84.41	54.60	70.25	77.66	78.32	87.19	90.66	84.89	85.27	56.46	69.23	74.13	71.56	66.06	76.03
CSL* [45]	R152-FPN	90.25	85.53	54.64	75.31	70.44	73.51	77.62	90.84	86.15	86.69	69.60	68.04	73.83	71.10	68.93	76.17
SCRDet+* [47]	R152-FPN	88.68	85.22	54.70	73.71	71.92	84.14	79.39	90.82	87.04	86.02	67.90	60.86	74.52	70.76	72.66	76.56
CFA* [13]	R-152	89.08	83.20	54.37	66.87	81.23	80.96	87.17	90.21	84.32	86.09	52.34	69.94	75.52	80.76	67.96	76.67
S ² A-Net* [15]	R50-FPN	88.89	83.60	57.74	81.95	79.94	83.19	89.11	90.78	84.87	87.81	70.30	68.25	78.30	77.01	69.58	79.42
ReDet* [16]	ReR50-ReFPN	88.81	82.48	60.83	80.82	78.34	86.06	88.31	90.87	88.77	87.03	68.65	66.90	79.26	79.71	74.67	80.10
Oriented R-CNN* [41]	R101-FPN	90.26	84.74	62.01	80.42	79.04	85.07	88.52	90.85	87.24	87.96	72.26	70.03	82.93	78.46	68.05	80.52
Point RCNN* (Ours)	ReR50-ReFPN	82.99	85.73	61.16	79.98	77.82	85.90	88.94	90.89	88.89	88.16	71.84	68.21	79.03	80.32	75.71	80.37
Point RCNN* [†] (Ours)	ReR50-ReFPN	86.21	86.44	60.30	80.12	76.45	86.17	88.58	90.84	88.58	88.44	73.03	70.10	79.26	79.02	77.15	80.71
Point RCNN* [†] (Ours)	Swin-T-FPN	86.59	85.72	61.64	81.08	81.01	86.49	88.84	90.83	87.22	88.23	68.85	71.48	82.09	83.60	76.08	81.32

Table 1. Performance comparisons on DOTA-v1.0 test set. * denotes multi-scale training and testing, [†] denotes the results of using balanced dataset strategy.

Method	Backbone	PL	BD	BR	GTF	SV	LV	SH	TC	BC	ST	SBF	RA	HA	SP	HC	CC	mAP (%)
RetinaNet-O [26]	R50-FPN	71.43	77.64	42.12	64.65	44.53	56.79	73.31	90.84	76.02	59.96	46.95	69.24	59.65	64.52	48.06	0.83	59.16
FR-O [40]	R50-FPN	71.89	74.47	44.45	59.87	51.28	68.98	79.37	90.78	77.38	67.50	47.75	69.72	61.22	65.28	60.47	1.54	62.00
Mask R-CNN [17]	R50-FPN	76.84	73.51	49.90	57.80	51.31	71.34	79.75	90.46	74.21	66.07	46.21	70.61	63.07	64.46	57.81	9.42	62.67
HTC [5]	R50-FPN	77.80	73.67	51.40	63.99	51.54	73.31	80.31	90.48	75.12	67.34	48.51	70.63	64.84	64.48	55.87	5.15	63.40
OWSR* [23]	R101-FPN	-	-	-	-	-	-	-	-	-	-	-	-	-	-	-	-	74.90
Oriented R-CNN* [41]	R101-FPN	87.20	84.67	60.13	80.79	67.51	81.63	89.74	90.88	82.21	78.51	70.98	78.63	79.46	75.40	75.71	39.69	76.45
ReDet* [16]	ReR50-ReFPN	88.51	86.45	61.23	81.20	67.60	83.65	90.00	90.86	84.30	75.33	71.49	72.06	78.32	74.73	76.10	46.98	76.80
Point RCNN* (Ours)	ReR50-ReFPN	83.40	86.59	60.76	80.25	79.92	83.37	90.04	90.86	87.45	84.50	72.79	77.32	78.29	77.48	78.92	47.97	78.74
Point RCNN* [†] (Ours)	ReR50-ReFPN	83.12	86.55	60.84	82.43	80.60	83.39	90.01	90.88	87.25	84.60	73.49	78.51	78.75	78.41	76.12	54.12	79.31
Point RCNN* [†] (Ours)	Swin-T-FPN	86.93	85.79	59.52	80.42	81.91	81.92	89.95	90.35	85.72	85.84	68.57	76.35	78.79	81.24	78.64	69.23	80.14

Table 2. Performance comparisons on DOTA-v1.5 test set. * denotes multi-scale training and testing, [†] denotes the results of using balanced dataset strategy.

Method	Backbone	mAP ₀₇ (%)	mAP ₁₂ (%)
RC2 [27]	VGG16	75.70	-
RRPN [31]	R101	79.08	85.64
R ² PN [52]	VGG16	79.60	-
RRD [24]	VGG16	84.30	-
RoI-Trans. [8]	R101-FPN	86.20	-
Gliding Vertex [42]	R101-FPN	88.20	-
R ³ Det [44]	R101-FPN	89.26	-
DRN [32]	H34	-	92.7
CenterMap [38]	R50-FPN	-	92.8
CSL [45]	R152-FPN	89.62	-
S ² A-Net [15]	R101-FPN	90.17	95.01
ReDet [16]	ReR50-ReFPN	90.46	97.63
Orient R-CNN [41]	R101-FPN	90.50	97.60
Point RCNN (Ours)	ReR50-ReFPN	90.53	98.53

Table 3. Performance comparisons on HRSC2016 test set. mAP₀₇ and mAP₁₂ indicate that the results are evaluated under VOC2007 and VOC2012 metrics(%) respectively. We report both results for fair comparisons.

4.4. Ablation Study

In this section, if not specified, all the models are trained only on the training and validation set with scale 1.0 for simplicity, and are tested using multi-scale testing. The metric mAP is evaluated on the DOTA-v1.5 test set and obtained by submitting prediction results to DOTA’s evaluation server.

4.4.1 Effect of PointRPN

To analysis the efficiency of PointRPN, we evaluate the detection recall of PointRPN on the validation set of DOTA-v1.5. For simplicity, we train the models on the training

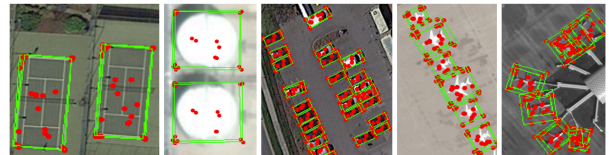


Figure 6. Examples of the learned points (red points) of PointRPN on DOTA-v1.0 test set. Green OBBs are the converted pseudo OBBs. The score threshold is set to 0.001 without NMS.

set with scale 1.0 and evaluate the metric recall on the validation set with scale 1.0 as well. The positive IoU threshold is set to 0.5. We select the top-300, top-1000, and top-2000 proposals to calculate their recall values and report the results in Tab. 4. We can find that when the proposals changes from top-2000 to top-1000, the recall value only drops 0.17%. Even if there are only top-300 proposals, the recall still achieves 85.93%.

Method	Recall ₃₀₀ (%)	Recall ₁₀₀₀ (%)	Recall ₂₀₀₀ (%)
PointRPN	85.93	89.83	90.00

Table 4. Comparison of the recall results by varying the number of proposals of each image patch. The metric recall is evaluated on the DOTA-v1.5 validation set.

4.4.2 Effect of Regression Type of PointReg

In this section, we analysis the effectiveness of the OBB regression type of PointReg. The results are shown in Tab. 5,

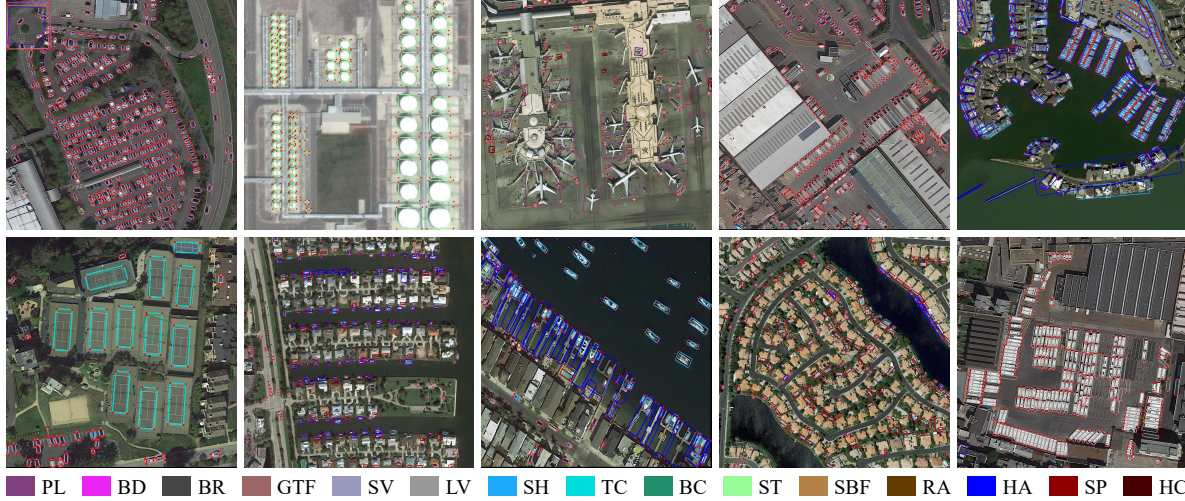


Figure 7. Visualization of the detection results of Point RCNN on DOTA-v1.0 test set. The score threshold is set to 0.01. Each color represents a category. The red points and colored OBBs are the predicted corner points and the converted OBBs of PointReg.

compared to the five-parameter representation, the eight-parameter regression type brings higher performance.

Regression type	mAP (%)
(x, y, w, h, θ)	77.25
$(x_1, y_1, x_2, y_2, x_3, y_3, x_4, y_4)$	77.60

Table 5. Analysis of the effectiveness of OBB regression type of PointReg. The metric mAP is evaluated on the DOTA-v1.5 test set.

4.4.3 Effect of Balanced Dataset

Oversampling threshold (β_{thr})	mAP (%)
0	73.52
0.1	76.49
0.2	77.44
0.3	77.60
0.4	77.48

Table 6. Comparison of detection accuracy by varying the oversampling threshold β_{thr} . The metric mAP is evaluated on the DOTA-v1.5 test set.

In this section, we analysis the impact of the oversampling threshold β_{thr} of the balanced dataset strategy. As shown in Tab. 6, we achieve the best detection accuracy of 77.60% at $\beta_{thr} = 0.3$. Therefore, we set $\beta_{thr} = 0.3$ in all other experiments on DOTA.

4.4.4 Factor-by-factor Experiment

To explore the effectiveness of each module of our proposed Point RCNN framework, we conduct a factor-by-factor experiment on the proposed PointRPN, PointReg and

Method	PointRPN	Balanced Dataset	PointReg	mAP (%)
Baseline				71.36
Point RCNN	✓			74.17
		✓		74.22
	✓	✓		77.25
	✓	✓	✓	77.60

Table 7. Factor-by-factor ablation experiments. The detection performance is evaluated on the test set of DOTA-v1.5 dataset.

balanced dataset strategy. The results are depicted in Tab. 7, each component has a positive effect, and all components are combined to obtain the best performance.

4.4.5 Visualization Analysis

We visualize some detection results on DOTA-v1.0 test set. Fig. 6 shows some examples of the learned points of PointRPN, which indicates that PointRPN is capable of learning representative points of rotated object. Fig. 7 shows some final detection results of Point RCNN, the red points denote the corner points learned by PointReg and the colored OBBs converted by the `MinAreaRect` function of OpenCV are the final results.

4.5. Limitations

Although experiments substantiate the superiority of Point RCNN over state-of-the-art methods, our method does not perform well enough in some categories, *e.g.*, PL (Plane), which needs to be further explored. Point RCNN also needs to use rotate NMS to remove duplicate results, which may mistakenly delete the TP. Transformer-based methods [4] may be the potential solutions, which will be the future work.

5. Conclusion

In this work, we revisit rotated object detection and propose a purely angle-free framework for rotated object detection, named Point RCNN, which mainly consists of a PointRPN for generating accurate RROIs, and a PointReg for refining corner points based on the generated RROIs. In addition, we propose a balanced dataset strategy to overcome the long-tailed distribution of different object classes in aerial images. Extensive experiments on several large-scale benchmarks demonstrate the significant superiority of our proposed framework against the state-of-the-arts.

References

- [1] Seyed Majid Azimi, Eleonora Vig, Reza Bahmanyar, Marco Körner, and Peter Reinartz. Towards multi-class object detection in unconstrained remote sensing imagery. In *Asian Conference on Computer Vision*, pages 150–165. Springer, 2018. 2, 3
- [2] G. Bradski. The OpenCV Library. *Dr. Dobb's Journal of Software Tools*, 2000. 2, 4, 5
- [3] Zhaowei Cai and Nuno Vasconcelos. Cascade r-cnn: Delving into high quality object detection. In *Proceedings of the IEEE Conference on Computer Vision and Pattern Recognition (CVPR)*, pages 6154–6162, 2018. 2
- [4] Nicolas Carion, Francisco Massa, Gabriel Synnaeve, Nicolas Usunier, Alexander Kirillov, and Sergey Zagoruyko. End-to-end object detection with transformers. In Andrea Vedaldi, Horst Bischof, Thomas Brox, and Jan-Michael Frahm, editors, *ECCV*, 2020. 8
- [5] Kai Chen, Jiangmiao Pang, Jiaqi Wang, Yu Xiong, Xiaoxiao Li, Shuyang Sun, Wansen Feng, Ziwei Liu, Jianping Shi, Wanli Ouyang, et al. Hybrid task cascade for instance segmentation. In *Proceedings of the IEEE/CVF Conference on Computer Vision and Pattern Recognition*, pages 4974–4983, 2019. 7
- [6] Kai Chen, Jiaqi Wang, Jiangmiao Pang, Yuhang Cao, Yu Xiong, Xiaoxiao Li, Shuyang Sun, Wansen Feng, Ziwei Liu, Jiarui Xu, Zheng Zhang, Dazhi Cheng, Chenchen Zhu, Tianheng Cheng, Qijie Zhao, Buyu Li, Xin Lu, Rui Zhu, Yue Wu, Jifeng Dai, Jingdong Wang, Jianping Shi, Wanli Ouyang, Chen Change Loy, and Dahua Lin. MMDetection: Open mmlab detection toolbox and benchmark. 2019. 6
- [7] Jifeng Dai, Haozhi Qi, Yuwen Xiong, Yi Li, Guodong Zhang, Han Hu, and Yichen Wei. Deformable convolutional networks. In *Proceedings of the IEEE international conference on computer vision*, pages 764–773, 2017. 4
- [8] Jian Ding, Nan Xue, Yang Long, Gui-Song Xia, and Qikai Lu. Learning roi transformer for oriented object detection in aerial images. In *Proceedings of the IEEE/CVF Conference on Computer Vision and Pattern Recognition*, pages 2849–2858, 2019. 1, 2, 4, 5, 6, 7
- [9] Jian Ding, Nan Xue, Gui-Song Xia, Xiang Bai, Wen Yang, Micheal Ying Yang, Serge Belongie, Jiebo Luo, Mihai Datcu, Marcello Pelillo, et al. Object detection in aerial images: A large-scale benchmark and challenges. *arXiv preprint arXiv:2102.12219*, 2021. 1, 6
- [10] Kaiwen Duan, Song Bai, Lingxi Xie, Honggang Qi, Qingming Huang, and Qi Tian. Centernet: Keypoint triplets for object detection. In *International Conference on Computer Vision (ICCV)*, pages 6569–6578, 2019. 2
- [11] Ross Girshick. Fast r-cnn. In *Proceedings of the IEEE International Conference on Computer Vision (ICCV)*, pages 1440–1448, 2015. 2
- [12] Ross Girshick, Jeff Donahue, Trevor Darrell, and Jitendra Malik. Rich feature hierarchies for accurate object detection and semantic segmentation. In *Proceedings of the IEEE Conference on Computer Vision and Pattern Recognition (CVPR)*, pages 580–587, 2014. 2
- [13] Zonghao Guo, Chang Liu, Xiaosong Zhang, Jianbin Jiao, Xiangyang Ji, and Qixiang Ye. Beyond bounding-box: Convex-hull feature adaptation for oriented and densely packed object detection. In *CVPR*, pages 8792–8801, June 2021. 3, 4, 7
- [14] Agrim Gupta, Piotr Dollár, and Ross B. Girshick. LVIS: A dataset for large vocabulary instance segmentation. In *CVPR*, 2019. 6
- [15] Jiaming Han, Jian Ding, Jie Li, and Gui-Song Xia. Align deep features for oriented object detection. *IEEE Transactions on Geoscience and Remote Sensing*, 2021. 1, 2, 6, 7
- [16] Jiaming Han, Jian Ding, Nan Xue, and Gui-Song Xia. Redet: A rotation-equivariant detector for aerial object detection. In *Proceedings of the IEEE/CVF Conference on Computer Vision and Pattern Recognition*, pages 2786–2795, 2021. 1, 2, 4, 5, 6, 7
- [17] Kaiming He, Georgia Gkioxari, Piotr Dollár, and Ross Girshick. Mask r-cnn. In *Proceedings of the IEEE international conference on computer vision*, pages 2961–2969, 2017. 2, 7
- [18] Han Hu, Jiayuan Gu, Zheng Zhang, Jifeng Dai, and Yichen Wei. Relation networks for object detection. In *Proceedings of the IEEE Conference on Computer Vision and Pattern Recognition (CVPR)*, pages 3588–3597, 2018. 2
- [19] Ray A Jarvis. On the identification of the convex hull of a finite set of points in the plane. *Information processing letters*, 2(1):18–21, 1973. 5
- [20] Yingying Jiang, Xiangyu Zhu, Xiaobing Wang, Shuli Yang, Wei Li, Hua Wang, Pei Fu, and Zhenbo Luo. R 2 cnn: Rotational region cnn for arbitrarily-oriented scene text detection. In *2018 24th International Conference on Pattern Recognition (ICPR)*, pages 3610–3615. IEEE, 2018. 1, 2
- [21] Diederik P. Kingma and Jimmy Ba. Adam: A method for stochastic optimization. In Yoshua Bengio and Yann LeCun, editors, *ICLR*, 2015. 6
- [22] Hei Law and Jia Deng. Cornernet: Detecting objects as paired keypoints. In *Proceedings of the European Conference on Computer Vision (ECCV)*, pages 734–750, 2018. 2
- [23] Chengzheng Li, Chunyan Xu, Zhen Cui, Dan Wang, Zequn Jie, Tong Zhang, and Jian Yang. Learning object-wise semantic representation for detection in remote sensing imagery. In *Proceedings of the IEEE/CVF Conference on Computer Vision and Pattern Recognition Workshops*, pages 20–27, 2019. 7
- [24] Minghui Liao, Zhen Zhu, Baoguang Shi, Gui-song Xia, and Xiang Bai. Rotation-sensitive regression for oriented scene

- text detection. In *Proceedings of the IEEE conference on computer vision and pattern recognition*, pages 5909–5918, 2018. 7
- [25] Tsung-Yi Lin, Piotr Dollár, Ross Girshick, Kaiming He, Bharath Hariharan, and Serge Belongie. Feature pyramid networks for object detection. In *Proceedings of the IEEE Conference on Computer Vision and Pattern Recognition (CVPR)*, pages 2117–2125, 2017. 2
- [26] Tsung-Yi Lin, Priya Goyal, Ross Girshick, Kaiming He, and Piotr Dollár. Focal loss for dense object detection. In *Proceedings of the IEEE international conference on computer vision*, pages 2980–2988, 2017. 2, 5, 7
- [27] Lei Liu, Zongxu Pan, and Bin Lei. Learning a rotation invariant detector with rotatable bounding box. *arXiv preprint arXiv:1711.09405*, 2017. 7
- [28] Wei Liu, Dragomir Anguelov, Dumitru Erhan, Christian Szegedy, Scott Reed, Cheng-Yang Fu, and Alexander C Berg. Ssd: Single shot multibox detector. In *European Conference on Computer Vision (ECCV)*, pages 21–37. Springer, 2016. 2
- [29] Ze Liu, Yutong Lin, Yue Cao, Han Hu, Yixuan Wei, Zheng Zhang, Stephen Lin, and Baining Guo. Swin transformer: Hierarchical vision transformer using shifted windows. *arXiv preprint arXiv:2103.14030*, 2021. 6
- [30] Zikun Liu, Liu Yuan, Lubin Weng, and Yiping Yang. A high resolution optical satellite image dataset for ship recognition and some new baselines. In *International conference on pattern recognition applications and methods*, volume 2, pages 324–331. SCITEPRESS, 2017. 6
- [31] Jianqi Ma, Weiyuan Shao, Hao Ye, Li Wang, Hong Wang, Yingbin Zheng, and Xiangyang Xue. Arbitrary-oriented scene text detection via rotation proposals. *IEEE Transactions on Multimedia*, 20(11):3111–3122, 2018. 1, 2, 7
- [32] Xingjia Pan, Yuqiang Ren, Kekai Sheng, Weiming Dong, Haolei Yuan, Xiaowei Guo, Chongyang Ma, and Changsheng Xu. Dynamic refinement network for oriented and densely packed object detection. In *Proceedings of the IEEE/CVF Conference on Computer Vision and Pattern Recognition*, pages 11207–11216, 2020. 7
- [33] Wen Qian, Xue Yang, Silong Peng, Yue Guo, and Junchi Yan. Learning modulated loss for rotated object detection. *arXiv preprint arXiv:1911.08299*, 2019. 2, 3
- [34] Joseph Redmon, Santosh Divvala, Ross Girshick, and Ali Farhadi. You only look once: Unified, real-time object detection. In *Proceedings of the IEEE Conference on Computer Vision and Pattern Recognition (CVPR)*, pages 779–788, 2016. 2
- [35] Shaoqing Ren, Kaiming He, Ross Girshick, and Jian Sun. Faster r-cnn: Towards real-time object detection with region proposal networks. In *Advances in Neural Information Processing Systems (NIPS)*, pages 91–99, 2015. 2
- [36] Shaoqing Ren, Kaiming He, Ross B. Girshick, and Jian Sun. Faster R-CNN: Towards real-time object detection with region proposal networks. In *NeurIPS*, 2015. 4
- [37] Zhi Tian, Chunhua Shen, Hao Chen, and Tong He. Fcos: Fully convolutional one-stage object detection. In *Proceedings of the IEEE International Conference on Computer Vision (ICCV)*, pages 9627–9636, 2019. 2
- [38] Jinwang Wang, Wen Yang, Heng-Chao Li, Haijian Zhang, and Gui-Song Xia. Learning center probability map for detecting objects in aerial images. *IEEE Transactions on Geoscience and Remote Sensing*, 59(5):4307–4323, 2020. 7
- [39] Haoran Wei, Yue Zhang, Zhonghan Chang, Hao Li, Hongqi Wang, and Xian Sun. Oriented objects as pairs of middle lines. *ISPRS Journal of Photogrammetry and Remote Sensing*, 169:268–279, 2020. 7
- [40] Gui-Song Xia, Xiang Bai, Jian Ding, Zhen Zhu, Serge Belongie, Jiebo Luo, Mihai Datcu, Marcello Pelillo, and Liangpei Zhang. Dota: A large-scale dataset for object detection in aerial images. In *Proceedings of the IEEE conference on computer vision and pattern recognition*, pages 3974–3983, 2018. 1, 6, 7
- [41] Xingxing Xie, Gong Cheng, Jiabao Wang, Xiwen Yao, and Junwei Han. Oriented r-cnn for object detection. *arXiv preprint arXiv:2108.05699*, 2021. 1, 2, 7
- [42] Yongchao Xu, Mingtao Fu, Qimeng Wang, Yukang Wang, Kai Chen, Gui-Song Xia, and Xiang Bai. Gliding vertex on the horizontal bounding box for multi-oriented object detection. *IEEE transactions on pattern analysis and machine intelligence*, 43(4):1452–1459, 2020. 2, 3, 7
- [43] Xue Yang, Liping Hou, Yue Zhou, Wentao Wang, and Junchi Yan. Dense label encoding for boundary discontinuity free rotation detection. In *CVPR*, 2021. 1, 3
- [44] Xue Yang, Qingqing Liu, Junchi Yan, Ang Li, Zhiqiang Zhang, and Gang Yu. R3det: Refined single-stage detector with feature refinement for rotating object. *arXiv preprint arXiv:1908.05612*, 2(4), 2019. 1, 7
- [45] Xue Yang and Junchi Yan. Arbitrary-oriented object detection with circular smooth label. In *European Conference on Computer Vision*, pages 677–694. Springer, 2020. 1, 2, 7
- [46] Xue Yang, Junchi Yan, Qi Ming, Wentao Wang, Xiaopeng Zhang, and Qi Tian. Rethinking rotated object detection with gaussian wasserstein distance loss. 2021. 2
- [47] Xue Yang, Junchi Yan, Xiaokang Yang, Jin Tang, Wenlong Liao, and Tao He. Scrdet++: Detecting small, cluttered and rotated objects via instance-level feature denoising and rotation loss smoothing. *arXiv preprint arXiv:2004.13316*, 2020. 1, 3, 7
- [48] Xue Yang, Jirui Yang, Junchi Yan, Yue Zhang, Tengfei Zhang, Zhi Guo, Xian Sun, and Kun Fu. Scrdet: Towards more robust detection for small, cluttered and rotated objects. In *Proceedings of the IEEE/CVF International Conference on Computer Vision*, pages 8232–8241, 2019. 1, 2
- [49] Xue Yang, Xiaojiang Yang, Jirui Yang, Qi Ming, Wentao Wang, Qi Tian, and Junchi Yan. Learning high-precision bounding box for rotated object detection via kullback-leibler divergence. 2021. 2
- [50] Ze Yang, Shaohui Liu, Han Hu, Liwei Wang, and Stephen Lin. Reppoints: Point set representation for object detection. In *Proceedings of the IEEE/CVF International Conference on Computer Vision*, pages 9657–9666, 2019. 2, 4
- [51] Jingru Yi, Pengxiang Wu, Bo Liu, Qiaoying Huang, Hui Qu, and Dimitris Metaxas. Oriented object detection in aerial images with box boundary-aware vectors. In *Proceedings of the IEEE/CVF Winter Conference on Applications of Computer Vision*, pages 2150–2159, 2021. 2, 3, 7

- [52] Zenghui Zhang, Weiwei Guo, Shengnan Zhu, and Wenxian Yu. Toward arbitrary-oriented ship detection with rotated region proposal and discrimination networks. *IEEE Geoscience and Remote Sensing Letters*, 15(11):1745–1749, 2018. [1](#), [2](#), [7](#)